Journal of Biomechanics 183 (2025) 112628

Contents lists available at ScienceDirect

Journal of Biomechanics

journal homepage: www.elsevier.com/locate/jbiomech

CFD and PIV analysis of a novel, low shear stress intra-aortic ventricular assist device

Elif Oran [a], Essam Abo-Serie [b,*], James Jewkes [b], Manus Henry [a,c], Bulent Oran [d]

[a] Coventry University, Centre for Fluid and Complex Systems, Coventry, UK
[b] University of Leicester, School of Engineering, Leicester, UK
[c] University of Oxford, Department of Engineering Science, Oxford, UK
[d] Medicana International Hospital, Department of Pediatric Cardiology, Izmir, Turkey

ARTICLE INFO

Keywords:
Left Ventricular Assist Device (LVAD)
Computational Fluid Dynamics (CFD)
Cardiovascular Mock Circulation Loop (CMCL)
Particle Image Velocimetry (PIV)
viscous shear stress (VSS)
LifeheART

ABSTRACT

Stroke has emerged as the primary contributor to morbidity and mortality in patients undergoing treatment with Left Ventricular Assist Devices (LVADs), possibly arising from the turbulent flow and elevated wall shear stresses generated in these devices. A minimally invasive LVAD (*LifeheART*) has been proposed to address these issues, employing an intra-aortic location and a shaftless impeller design. The current study uses Particle Image Velocimetry (PIV) flow visualization, carried out in a Cardiovascular Mock Circulation Loop (CMCL), to identify the velocity distribution at the pump outlet in order to validate the developed CFD model. Subsequently, the model evaluates the blood shear stress distribution and blood damage index. The results showed that the calculated viscous shear stress (VSS) and the blood damage index of the *LifeheART* prototype is significantly lower than the published data for current clinically available devices, confirming the potential utility of the new design to improve patient outcomes.

1. Introduction

Advanced heart failure is associated with significant reductions in life expectancy, functional status, and quality of life. Left ventricular assist devices (LVADs) offer a therapeutic option, providing circulatory support for patients awaiting heart transplantation, or as a permanent "destination therapy" (Rogers et al., 2017). However, further improvements in efficacy and safety are urgently required (Starling et al., 2014; Kirklin et al., 2014).

LVAD use is associated with hemocompatibility-related complications such as thrombosis, stroke, and bleeding, resulting from adverse interactions between the pump and blood components (Thamsen et al., 2020; Oran et al., 2017; Inamullah et al., 2021). Currently the most widely implanted LVADs, the HeartMate II (HM II) (https://www.abbott.com) and HVAD (https://www.medtronic.com), have two-year survival rates of 57.4 % and 55 % respectively (Rogers et al., 2017). The HeartMate 3 (HM III) (https://www.abbott.com) was developed to increase survival rate and reduce complications by addressing some of the known issues, and is currently the most widely used LVAD in clinical settings. It features wide blood-flow pathways, friction-free movement and intrinsic pulsatility, replacing the HM II's axial pump with a centrifugal pump design. These innovations are designed to mitigate shear stress and blood stasis and have been found in clinical studies to provide enhanced patient outcomes (Mehra et al., 2018; Chiang et al., 2020). Mehra et al compared outcomes for 512 HM II patients and 516 HM III users. Over a two-year period, the survival rate without stroke was notably higher among patients using the HM III (76.9 %) compared to the HM II (64.8 %). The centrifugal pump design of the HM III was found to generate a lower shear stress distribution and a correspondingly lower hemolysis index compared to other HVAD devices (Wiegmann et al., 2019).

Our previous paper (Oran et al., 2024) describes a new intra-aortic and shaftless LVAD design, *LifeheART*, intended to be implanted in the aorta, intended to further reduce shear stress and hemolysis. The design geometry was optimised to deliver the required pump performance, CFD simulations were carried out, and pump performance was verified using experiments on a prototype device. Here we examine the performance in more detail using CFD tools and Particle Image Velocimetry (PIV) experiments to investigate blood damage characteristics. Results indicate that *LifeheART* generates reduced hemolysis and shear stress due to its wider blood-flow pathways, lower rotation speed and its intra-aortic placement.

* Corresponding author.
E-mail address: e.aboserie@leicester.ac.uk (E. Abo-Serie).

https://doi.org/10.1016/j.jbiomech.2025.112628
Accepted 10 March 2025
Available online 11 March 2025

The CFD analysis is undertaken in two stages:

- Firstly, the distribution of shear stress within the intra-aortic pump is investigated. Following the methodology of Fraser et al. (2012), the results are categorised by different shear stress levels, including a level below which no blood trauma is assumed. This analysis helps identify critical regions within the device where blood damage is most likely to occur.
- Secondly, the blood residence time is computed for the device regions. By determining how long blood elements remain within the regions, we can estimate the likelihood and extent of blood damage.

The model results have been validated via experimental work on a cardiovascular mock circulatory loop (CMCL), using PIV measurements to verify the predicted flow distribution at the LVAD exit. Finally, the performance is compared with published results from academic studies conducted on the HM II, HVAD, and HM III devices.

2. Materials and methods

2.1. Model geometry

The novel LVAD (*LifeheART*) is designed for placement within the aortic root using a stent (Fig. 1), and is configured as an axial pump, with no central shaft within the impeller. This minimally invasive implantation technique offers patients safer procedures with faster recovery and fewer complications (Wachter et al.,2019).

The *LifeheART* 's structure comprises a five-blade flow strainer at the inlet and a three-blade hub-less diffuser at the outlet. The impeller has a diameter of 30 mm and a length of 12 mm (Fig. 2). A preliminary investigation was conducted to determine the optimal blade geometry, as described by Oran et al. (2017). However, in this prior study, the distance between the rotor and stator of the electric motor was not considered, as the primary objective was to optimize blade parameters. In the current study, a shrouded rotor configuration is included in the design, incorporating a ring of magnets around the rotating blades, with a fixed gap between the rotor and stator. Other design dimensions are unchanged from Oran et al., 2024.

In vitro, the hydro-dynamically and magnetically levitated rotor passively adapts its position to achieve balance. For the purposes of this study, the distance between the rotor and stator was fixed at approximately 500 μm when incorporated into a prototype *LifeheART* LVAD operating in the range 2400 to 3200 rpm.

2.2. Computational simulations

CFD analyses were conducted using the commercial solver StarCCM+ (Siemens Digital Industries Software). Mesh generation was automated, incorporating surface, polyhedral, and prism layers. The flow domain was divided into approximately 18 million cells and adequate grid refinements were provided at the walls to resolve the near-wall flow. A mesh independence study was carried out, indicating that the difference in pressure rise between the finest and second finest grids was less than 0.1 %. At all the wall surfaces the prism layer was refined to ensure the y + value is less than 1.0 to accurately calculate the wall shear stress. The working fluid was characterized using the properties of human blood at 37 °C, assuming it to be an incompressible Newtonian fluid due to the high shear rates inherent in axial pumps (Burgreen et al., 2023; Puhan, 2021; Chaichana et al., 2012; Nammakie et al., 2017).

The inlet boundary conditions assumed a constant mass flow rate. The flow rate values were directly collected from the test rig during the experiments, ensuring consistency between the experimental and computational setups. The simulations were performed using flow rates corresponding to five different pump rotational speeds (RPM), enabling a comprehensive analysis of the device's performance across various operating conditions. The downstream boundary condition was set as an outlet to enable the pressure outlet to be evaluated. This boundary condition means the pressure gradient at the exit along the axis is zero. For this boundary condition to be valid we added a longer pipe at the exit of the pump to ensure the flow is fully developed. The widely used k-ε model was selected as the turbulence model for the numerical simulations (Thamsen et al., 2019). A moving reference frame was utilized to simulate the movement of the rotor (Silva et al., 2021; Khoo et al., 2018).

A key advantage of the intra-aortal location is the reduction in the required pressure duty compared with conventional devices. A typical duty for a LVAD is to deliver 4.5 L/min with a pressure rise of 80 mm Hg. This assumes zero input pressure, as the LVAD receives blood flow from the ventricle. *LifeheART* is positioned within the aorta, where the pressure varies between 80 and 120 mmHg throughout the cardiac cycle (Dewi et al., 2020; Mori et al.,2019; Guyton, 1973). Accordingly, the inlet pressure is assumed to have a minimum v'alue of 80 mmHg, and the role of the *LifeheART* is to reduce the pressure demand on the heart by providing sympathetic and dynamic support throughout the cardiac cycle. Thus *LifeheART* is required to provide 4.5 L/min with a maximum of only 40 mm Hg pressure rise to perform the same role as a

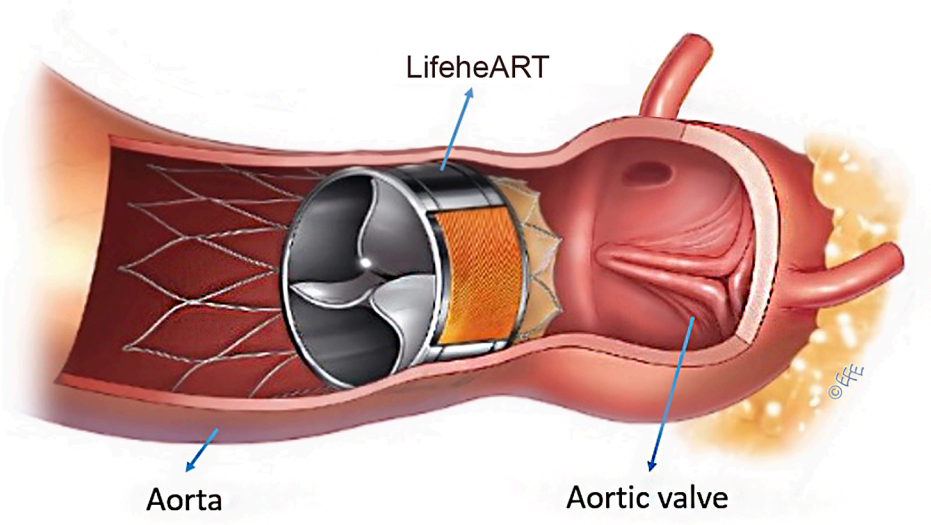

Fig. 1. The Intra-aortic LVAD (LifeheART) concept.

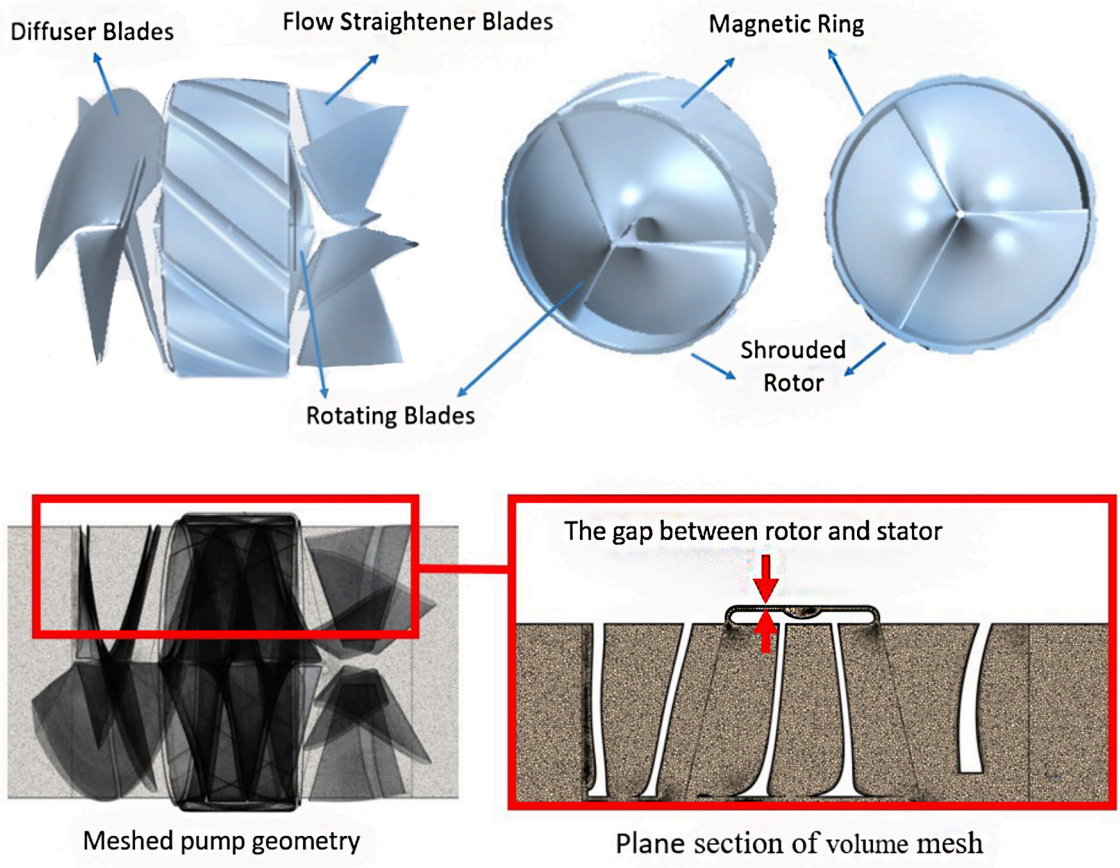

Fig. 2. CAD models of the LifeheART LVAD (top left) and the shrouded rotor of LifeheART (top right); details of the meshed LifeheART pump geometry (bottom left) and volume mesh plane section (bottom right).

conventional LVAD.

2.3. PIV experimental setup

Particle Image Velocimetry (PIV) has been employed at the outlet of a *LifeheART* prototype to provide flow visualization within a constant-flow cardiovascular mock loop (MCL). The experimental configuration includes several components, such as the pump prototype, a transparent acrylic observation area, tubing, and a reservoir. The equipment is shown in Fig. 3.

To keep the pump outlet pressure constant, a fixed-height tube creating a pressure drop of 40 mmHg has been added to the pump outlet. Tests were performed for flow rates between 3.5 and 7 l/min.

The test setup includes a *LifeheART* prototype with a flow line diameter of 30 mm placed inside a reservoir (Fig. 3b), forming a closed loop with steady-state flow conditions. The pump pushes fluid upward by creating pressure rise at its exit. Once the fluid reaches the top of the flow circuit, it returns to the reservoir. To regulate flow distribution, the entrance section of the reservoir is filled with glass marbles. The pump rotation speed is adjusted using a potentiometer connected to the motor driver, and the rotation speed is measured using data collected from hall effect sensors via an oscilloscope.

Glycerine (35 %) and water (65 %) were mixed to produce a solution with a kinematic viscosity similar to blood (3.5×10^{-3} Pa). Sodium iodide (NaI) was introduced to the solution to align its refractive index and avoid light path and image distortion (Xu et al., 2015; Medvitz et al., 2009). A semi-micro viscometer (Cannon-Manning model Viscolite 700, Hydramotion Co., UK), calibrated with pure water at room temperature, determined the working fluid viscosity to be 3.5 ± 0.2 cSt, i.e. a deviation of less than 1 % compared to the established standard value for blood. Silver-coated glass micro particles with a diameter of 10 μm were introduced into the flow upstream of the prototype pump.

The Dantec Dynamics PIV system comprises the operating software DaVis 10, a CMOS camera (LaVision Inc., Germany), and a Nano PIV YAG laser (Litron Co., UK) with output energies up to 425 mJ per pulse at 532 nm. Images were captured by the Lavision CMOS Imager CX-5 camera, paired with a Nikon 60 mm AF Micro NIKKOR lens, delivering a 2448 × 2048 pixel resolution and a pixel size of 2.7 μm. The PIV setup uses a Programmable Timing Unit (PTU) to synchronize the camera and laser. A double-frame double-pulse laser mode is utilized to produce two consecutive laser sheets across the centre of the transparent section at the pump outlet, resulting in two successive images depicting particle positions, using t = 800 μs. During each experiment, the Field Of View (FOV) of the images is 30 x 30 mm. The location of particles in each pair of images is used to calculate velocity vectors. Using established statistical analysis and cross correlations, a single velocity vector is used for each interrogation window (Ghodrati et al., 2021; Raffel et al., 2018).

3. Results

To compare the pump performance predicted by CFD and experimental results, the pump pressure rise predicted by the CFD model is compared with the experimental fixed pressure rise of 40 mmHg, using the same rotational speed and flow rates as determined experimentally. As shown in the Fig. 4, the CFD model predicts a pressure rise that is less than 5 % lower than the experimental value at all the tested speeds. The difference remains nearly the same under the pump nominal operating conditions (40 mmHg and 5 L/min) which occurs at pump speed 2800 rpm. PIV images were taken at a distance of 10 mm beyond the pump outlet. The velocity vector at each interrogation window was calculated from each pair of images and then results from 1000 image pairs were

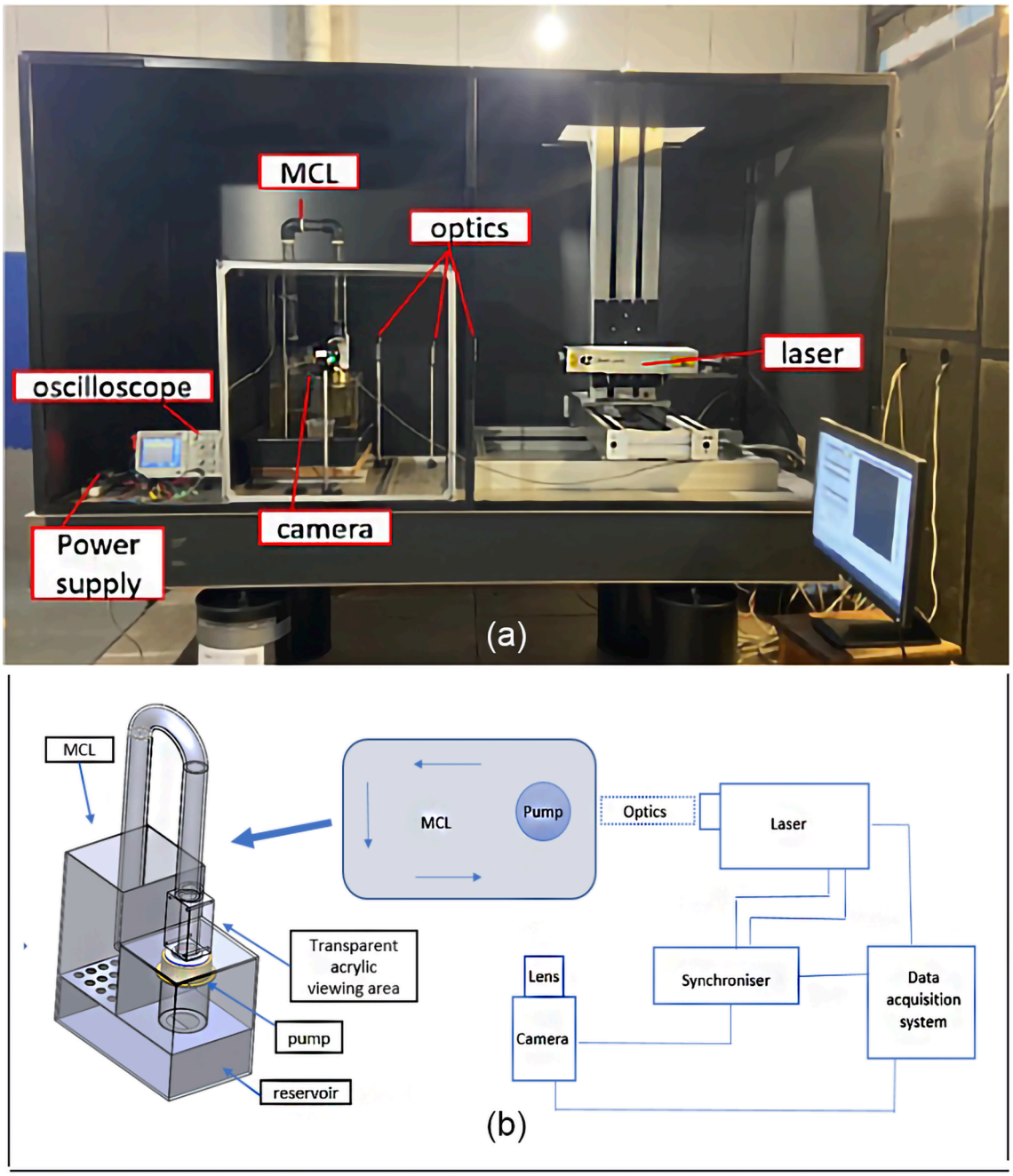

Fig. 3. (a) Photo and (b) Schematic diagram of the experimental setup used to conduct the PIV measurements on the LifeheART prototype.

averaged to evaluate the mean velocity. Fig. 5 presents only the resultant velocity of the axial and radial velocity components to enable comparison of the CFD model results with the PIV measurements, which show only 2D velocity vectors. The test results were obtained at five different pump speeds to demonstrate how the flow velocity changes. As the pump speed increased, the fluid velocity also increased, illustrating the direct relationship between rotational speed and fluid velocity within the pump. Fig. 5 also provides a visual representation of how the flow dynamics changed with varying pump speeds.

It was observed that the speed of the fluid was higher at the outer walls and decreased as it approached the centre. This is attributed to the high momentum provided by the pump blades as the liquid moves away from the blade centre, as well as the centrifugal forces induced by flow rotations. Note that the velocity shown here is the resultant of axial and radial velocities and does not include the tangential velocity component; also, the average axial velocity at any section remains the same by mass conservation. At lower rotational speeds (2400 rpm), the fluid movement is slower. As the speed increases to 3200 rpm, there is a significant increase in fluid velocity. These observations are important for understanding the pump's performance under different operating conditions. By maintaining a constant pressure rise, we can isolate the effect of rotational speed on fluid velocity, ensuring that any observed changes are due to speed variations rather than pressure fluctuations.

The PIV results for five different rotation speeds of the pump were compared with CFD analyses simulating the same conditions. To have a quantitative comparison of the flow velocity between experimental (PIV) and numerical (CFD) at the LifeheART pump exit for 2800 rpm, the flow velocity of the PIV and CFD results is averaged over the FOV length (30 mm) at each radial position from 0 mm at the wall to 15 mm at the pipe centre. Furthermore, the PIV mean value and standard deviation

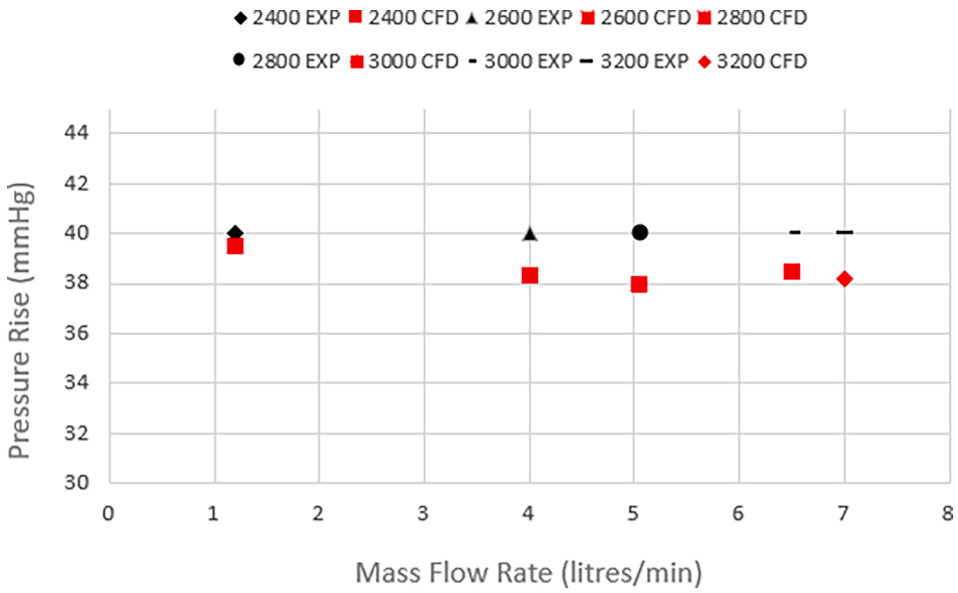

Fig. 4. Comparison of Experimental and CFD Results for Pressure Rise vs. Mass Flow Rate at Various Speeds (2400–3200 rpm).

are evaluated based on 1000 images. As shown in Fig. 6, the flow velocity trend is captured by the CFD model, including the peak value. However, near the pipe centreline, the predicted flow velocity is higher than that from the PIV measurements. The mean value and standard deviation of the PIV velocity, represented by the shaded blue line, reach their maximum values 1 mm away from the pipe wall due to the swirling exit flow. By shifting the FOV region on the CFD by further 10 mm and 25 mm away from the pump exit, it is noticed that the CFD velocity profile became closer to PIV measurements as shown in Fig. 6b and 6c. The differences between CFD and PIV results arise from uncertainties and CFD model assumptions. Validation on MCL involves quantifying the differences between experimental and simulation predictions. Both sources are influenced by distinct types of uncertainties, including model assumptions, measurement inaccuracies, and computational limitations (Santiago et al., 2022). Fig. 6 highlights the overall agreement between the two methods, capturing the velocity peak and decay. However, slight discrepancies at the centre underscore the challenges of accurately resolving complex flow interactions such as shear layers and recirculating vortices.".

The combined use of PIV measurements and CFD analyses have demonstrated that the new intra-aortic LifeheART LVAD design performs as expected, with reliable predictions of fluid velocity and pressure rise across different rotational speeds. Furthermore, a strong backflow in the central area of the diffuser was identified.

Fig. 7 illustrates the Wall Shear Stress (WSS) distributions on the impeller surface for each of the five rotational speeds of the *LifeheART* pump. At 4.5 L/min, the maximum WSS appears at the trailing edge of the flow straightener, particularly near the tip. Additionally, relatively high WSS values are observed at the trailing edge of the rotor centre.

4. Discussion

The CFD investigation was conducted on the new intra-aortic *LifeheART* LVAD pump, which enables minimally invasive surgical procedures. The computational model used for this study was validated using in-vitro experimental PIV data obtained from a cardiovascular mock loop. The comparison between CFD and PIV revealed a good correspondence regarding the overall velocity distribution within the flow fields at the pump exit. The results suggest that this innovative device may not only enhance patient recovery and reduce surgical risks but also achieve significantly lower hemolysis indices. As a result, it holds the potential to improve overall patient outcomes and reduce healthcare costs and device side effects.

Zhang et al. (2020) show the wall shear stress (WSS) and report the percentage of the impeller surface area with wall shear stress (WSS) exceeding 100 Pa and 500 Pa respectively for the two clinically widely used pumps (*HVAD and HM II)*, comparing these results with those obtained for their own new maglev centrifugal VAD (CH-VAD) under the same conditions as shown in Fig. 8.

The *LifeheART* demonstrates significantly lower WSS compared to the other three pumps. The CH-VAD, which is recognized for having the lowest WSS among current used devices and shares a similar geometry to the HeartMate 3 examined in other studies (Wiegmann et al., 2019; Thamsen et al., 2020), has a WSS value about twice as high as that of the *LifeheART* device. Furthermore, the *LifeheART* exhibits substantially lower percentages of its surface area having WSS values above 100 Pa and 500 Pa. Specifically, only 7.49 % of the new device's area has a WSS value above 100 Pa, compared to 13.7 % for the CH-VAD, 42.2 % for the HVAD, and 47.1 % for the HM II. Additionally, the *LifeheART* area with a WSS value above 100 Pa is approximately half that of the CH-VAD. For WSS values exceeding 500 Pa, the *LifeheART* also has a significantly reduced area compared to the CH-VAD, with values of 0.056 % for the *LifeheART* device versus 0.4 % for the CH-VAD.

Thamsen and colleagues conducted a study that evaluated the viscous sheer stress (VSS) of HM II and HVAD devices using volumetric histograms (Thamsen et al., 2015). The VSS values of the *LifeheART* device were then incorporated into these histograms for comparative analysis at normal performance conditions (80 mmHg and 4.5 L/min) (Fig. 8). In our analysis, we evaluated the VSS at 4.5 L/min and a pressure of 120 mmHg which is higher than that used to study the other devices (80 mmHg). Given that the *LifeheART* is positioned within the aorta, we used this pressure level as the benchmark for calculating the maximum stress values that the device can generate.

Fig. 9 shows the VSS values of current devices under normal performance conditions (80 mmHg and 4.5 L/min) together with the VSS values of the *LifeheART* LVAD under maximum performance conditions. The *LifeheART* demonstrates significantly lower VSS under maximum operating conditions, while the three other devices exhibit higher VSS values when operating at lower pressure.

In Thamsen et al.'s study, the volume of blood exposed to various levels of viscous shear stress within the LVADs (HM II and HVAD) were analyzed in the light of known VSS thresholds for blood damage (Thamsen et al., 2015). These thresholds were 9 Pa for von Willebrand factor (vWF) damage, 50 Pa for platelet activation, and 150 Pa for

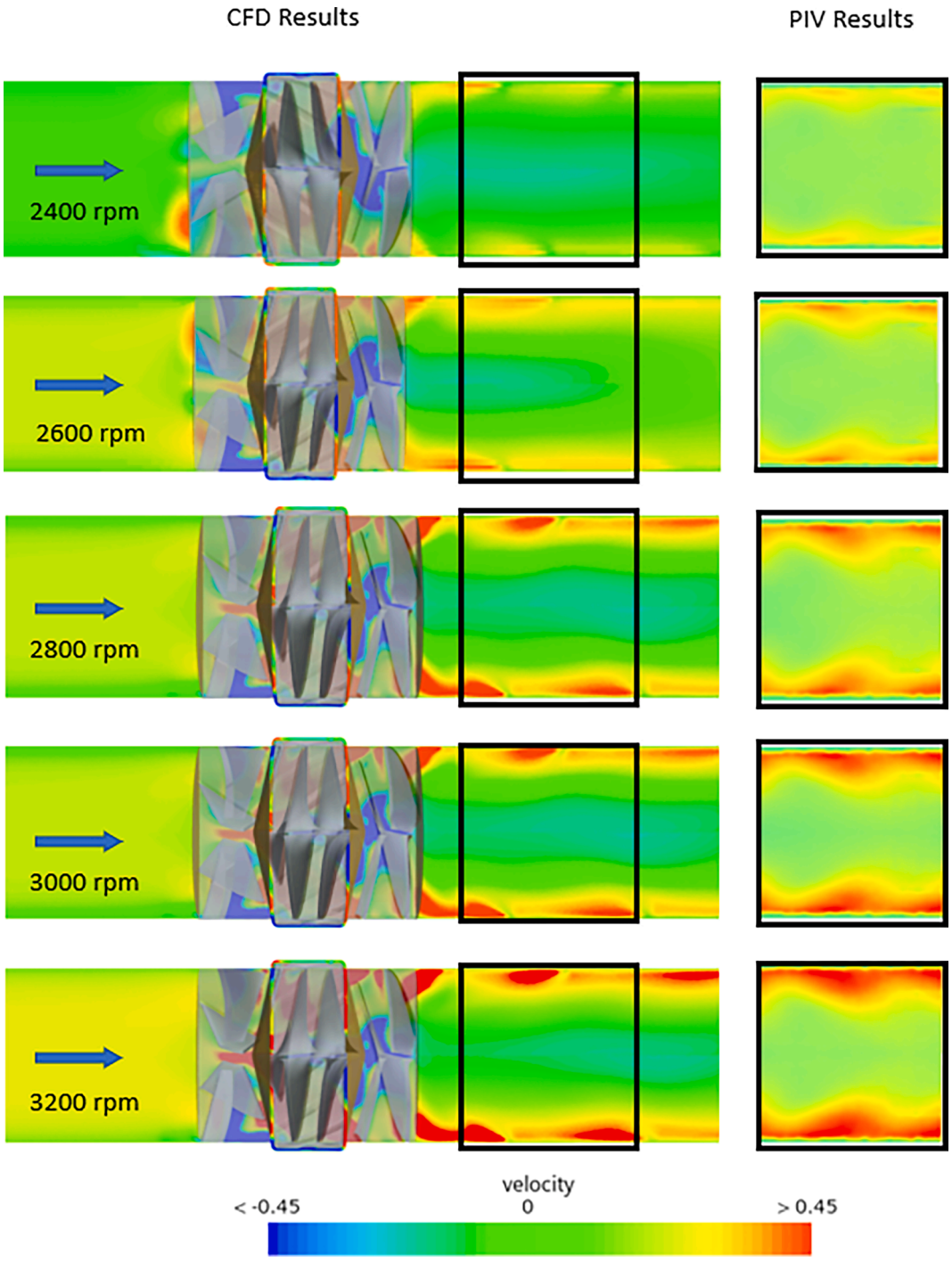

Fig. 5. Radial and Axial Velocity Distribution at the LifeheART Pump Exit: Comparison Between PIV Experiments and CFD Simulations.

hemolysis. The findings revealed that the HVAD pump has a larger surface area where blood is exposed to shear stresses exceeding the 9 Pa threshold, indicating a higher potential for vWF damage compared to other pumps. For platelet activation, while the clinically two tested pumps showed similar volume exposed to same stress, the *LifeheART* design showed less than half of these values, suggesting a lower risk for platelet activation. Similarly, for hemolysis, the LifeheArt design has a small volume exceeding 150 Pa compared to the other devices.

In addition, the LifeheART pump exhibited significantly lower cell residence times at all shear stress thresholds, meaning that blood cells spend less time in high shear stress regions. This shorter residence time potentially decreases the risk of blood damage from the LifeheART. Overall, while existing devices have comparable risks for platelet activation and hemolysis, the LifeheART shows lower risks for these conditions.

In Thamsen et al.'s study, hemolysis indices for HVAD and HM II were calculated using the Eulerian approach based on Goubergrits' methodology (Goubergrits, 2006). The results revealed nearly identical hemolysis indices, with values of 3.75 × 10–5 for the HVAD and 3.85 × 10–5 for the HM II. By contrast, the hemolysis index calculated for LifeheART device is significantly lower at 1.21 × 10–5, even for the maximum pressure duty. Overall, these results suggest that the new intra-aortic pump has the potential to operate with a significantly reduced hemolysis risk.

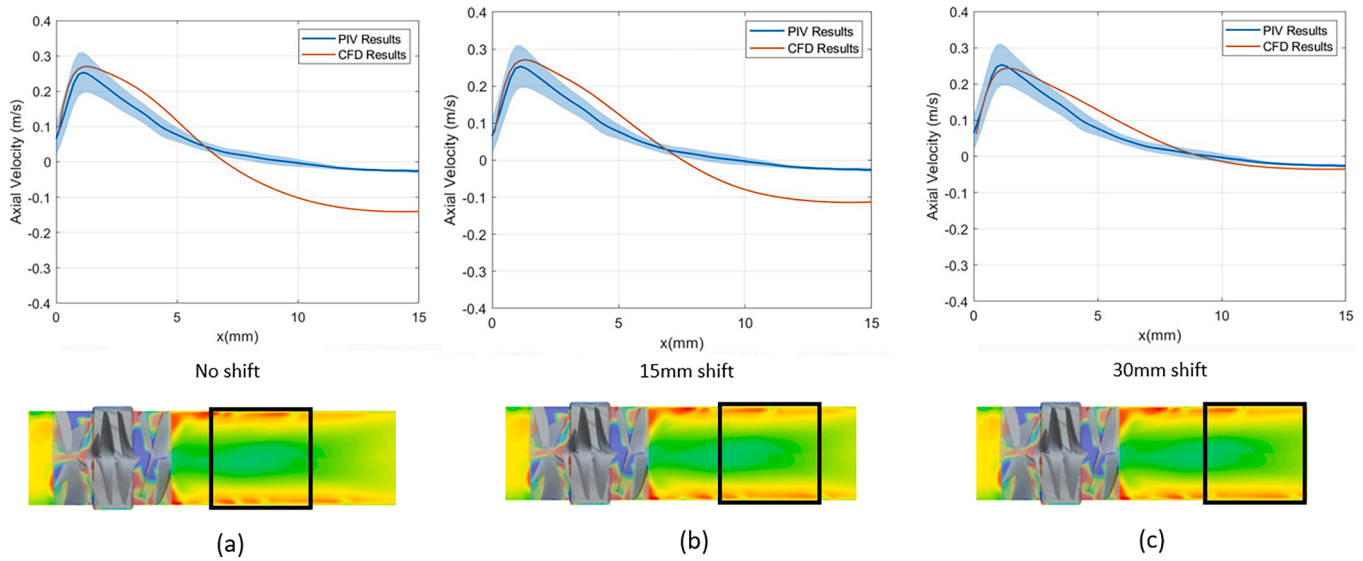

Fig. 6. Comparison of the CFD resultant velocity (Radial and Axial) at 10 (no shift), 25 (15 mm shift) and 40 mm (30 mm shift) with PIV measurements at 10 mm from the LifeheART Pump Exit (2800 rpm).

Elevated stresses impact erythrocytes, platelets, leucocytes, and blood proteins, leading to hemolysis, platelet activation, and impairment of vWF function. Experimentally determined stress thresholds for hemolysis are typically above 150 Pa and depend on exposure time (Quinlan et al., 2007). However, even subclinical hemolysis, occurring below these thresholds, can contribute to thrombotic adverse events (Bartoli et al., 2018). HM III is reported as having the lowest viscous stress value among the clinically used LVAD devices (Gil et al., 2023; Wiegmann et al., 2019). Its viscous stresses are generally kept below 150 Pa under tested conditions. However, despite these lower stress values, the short-term rates of stroke and gastrointestinal bleeding remain unchanged (Krabatsch et al., 2017; Mehra et al., 2017). This suggests that not only viscous stresses above 150 Pa but also those below 150 Pa remain significant concerns in LVADs and need to be further reduced. The *LifeheART* has low viscous stress values compared to other devices, and therefore can be a potential solution to the above-mentioned side effects.

The results also suggest that, while the current devices perform similarly regarding platelet activation and hemolysis risks, the *LifeheART* offers lower risks for these conditions. Conversely, the HVAD pump may present a higher risk of vWF damage and prolonged cell exposure to high shear stress. Additionally, the *LifeheART* pump demonstrated significantly lower residence times at all shear stress thresholds, implying that blood cells spend less time in regions with elevated shear stress. This could potentially decrease the risk of damage, a situation that also applies to higher shear stresses associated with hemolysis.

This study has several limitations. The PIV measurements are also focused on axial and radial velocity due to the difficulty to measure the tangential components. Although aortic distensibility and anatomy was not considered, the use of a continuous flow LVAD helps to minimize the variations in arterial wall deformation, thereby partially mitigating this limitation. We acknowledge that the validation is not comprehensive, as comparisons inside the device were not included. This limitation arises from the practical challenges of using PIV to measure highly constrained and opaque internal geometries. However, the CFD results both within and outside the device, combined with the distal PIV measurements, contribute towards a broader understanding of the device's behaviour. A Hall effect current sensor was employed to measure the pump speed. The reported error rate for this measurement is $\pm$ 2 %, which could introduce some degree of variability or inaccuracy in the results. Additionally, we simplified our CFD model by modelling blood as a Newtonian fluid similar to previous studies.

5. Conclusion

The study conducted on a novel intra-aortic, LVAD, *LifeheART*, demonstrates significant potential for reducing blood damage risks commonly associated with existing LVAD technologies. Through CFD analysis and PIV experiments, the *LifeheART* device shows reductions in both wall shear stress and viscous shear stress compared with three clinically tested devices, indicating a potential reduction in complications such as hemolysis, platelet activation, and von Willebrand factor damage. The shaftless impeller design and intra-aortic placement effectively lower blood residence times in high shear regions, further mitigating risks of blood trauma. The computational results demonstrate a significantly reduced hemolysis index for the LifeheART device compared to other devices. However, future work will include in vitro hemolysis testing to validate the computational model and provide experimental evidence to further support these findings. The method used to calculate the blood damage index is well-established for comparing heart assist devices; however, this method does not account for the location of blood damage within the domain. Further analysis is required to identify the location of vortices and retention time using techniques such as VolRec (Martorell et al., 2014; De Nisco et al., 2020).

Overall, the *LifeheART* intra-aortic LVAD could potentially lower the incidence of thrombotic events, stroke, and other adverse outcomes, paving the way for safer and more effective cardiac support devices.

CRediT authorship contribution statement

Elif Oran: Writing – review & editing, Writing – original draft, Visualization, Software, Methodology, Investigation, Funding acquisition, Formal analysis, Data curation, Conceptualization. **Essam Abo-Serie:** Writing – review & editing, Validation, Supervision, Software, Resources, Methodology, Investigation, Formal analysis. **James Jewkes:** Writing – review & editing, Visualization, Supervision, Software, Formal analysis. **Manus Henry:** Writing – review & editing, Supervision, Resources, Project administration, Investigation, Data curation. **Bulent Oran:** Writing – review & editing, Visualization, Supervision, Resources, Funding acquisition, Conceptualization.

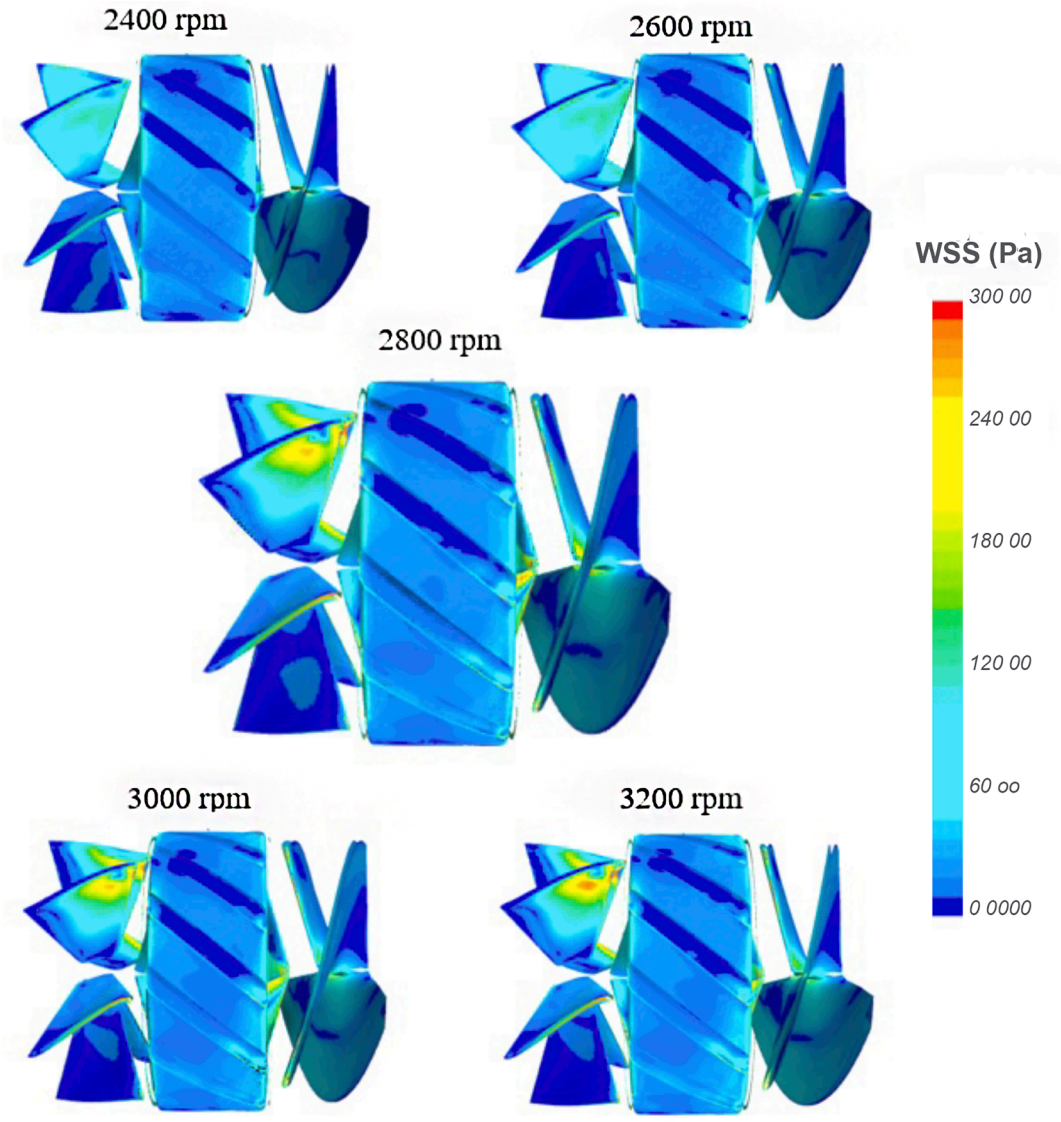

Fig. 7. Wall Shear Stress (WSS) distribution on the LifeheART geometry for different rotational speeds.

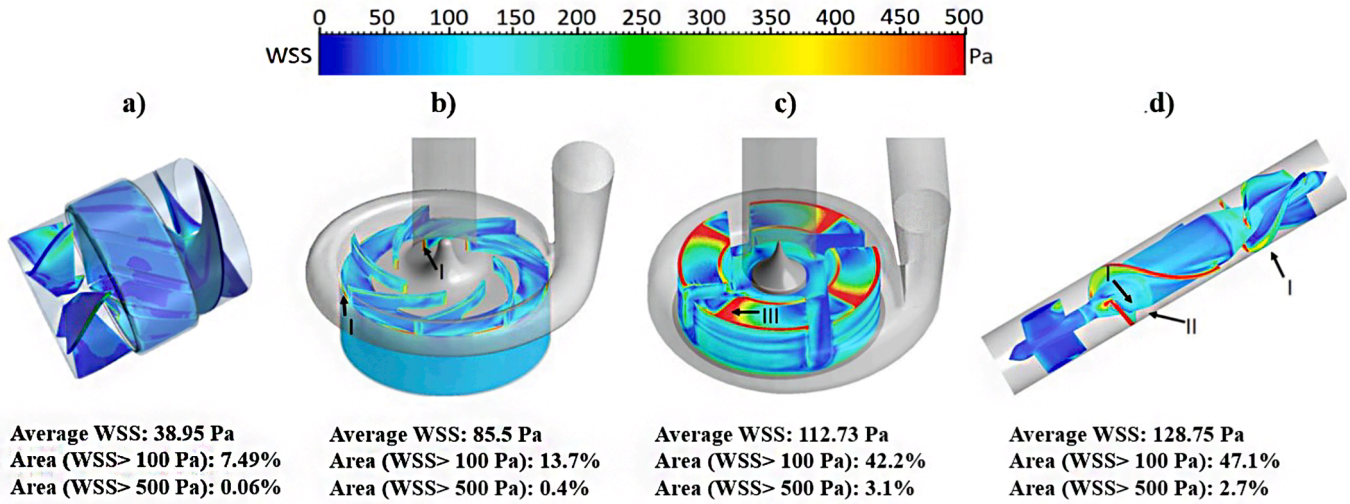

Fig. 8. Illustrates the distribution of wall shear stress (WSS) on the impeller surfaces with an aortic pressure of 120 mmHg: (a) LifeheART from this study; (b) CH-VAD; (c) HVAD; and (d) HM II, as reported by Zhang et al. (2020).

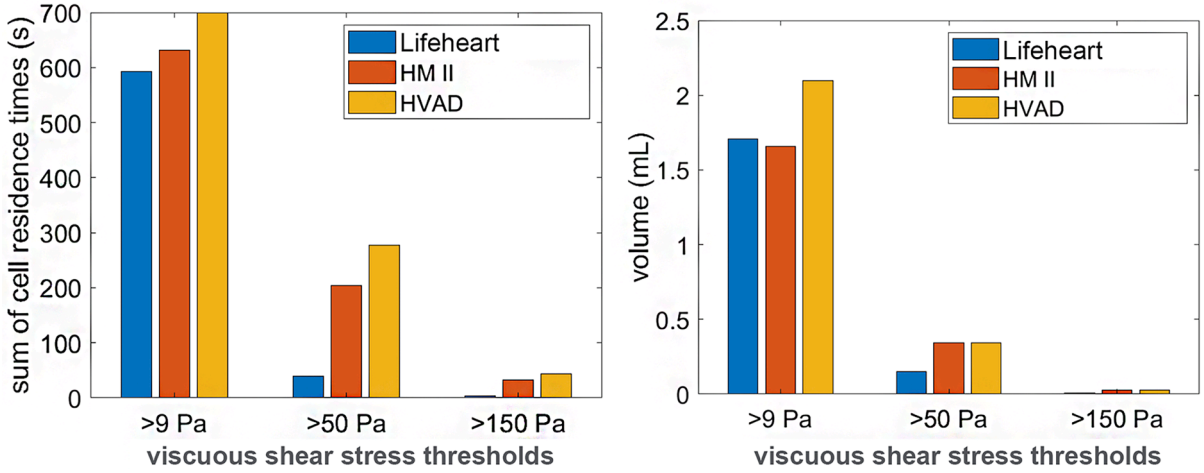

Fig. 9. Comparing the viscous shear stress (VSS) distribution in LifeheART with current data of other devices which published by Thamsen et al., (2015).

Declaration of competing interest

The authors declare that they have no known competing financial interests or personal relationships that could have appeared to influence the work reported in this paper.

Acknowledgements

The authors would like to acknowledge the financial support provided by Coventry University UK, University of Leicester UK: MRC-IAA Funding, RM61G1041M, and Misal Limited Company.

References

Bartoli, C.R., Zhang, D., Kang, J., Hennessy-Strahs, S., Restle, D., Howard, J., Redline, G., Bermudez, C., Atluri, P., Acker, M.A., 2018. Clinical and in vitro evidence that subclinical hemolysis contributes to LVAD thrombosis. Ann. Thorac. Surg. 105 (3), 807–814.

Burgreen, G.W., Zhussupbekov, M., Rojano, R.M. and Antaki, J.F., 2023. Exploratory Simulation of Thrombosis in a Temporary LVAD Catheter Pump within a Virtual In-vivo Left Heart Environment. ArXiv, pp.arXiv-2312.

Chaichana, T., Sun, Z., Jewkes, J., 2012. Computational fluid dynamics analysis of the effect of plaques in the left coronary artery. Comput. Math. Methods Med. 2012, 504367. https://doi.org/10.1155/2012/504367.

Chiang, Y.P., Cox, D., Schroder, J.N., Daneshmand, M.A., Blue, L.J., Patel, C.B., DeVore, A.D., Bishawi, M., Milano, C.A., 2020. Stroke risk following implantation of current generation centrifugal flow left ventricular assist devices. J. Card. Surg. 35 (2), 383–389.

Dewi, D.E.O., Yusof, N.S.M., 2020. Tissue-mimicking materials for cardiac imaging phantom—section 1: from conception to materials selection. Cardiovascular Engineering: Technological Advancements, Reviews, and Applications 3–33.

De Nisco, G., Gallo, D., Siciliano, K., Tasso, P., Rizzini, M.L., Mazzi, V., Calò, K., Antonucci, M., Morbiducci, U., 2020. Hemodialysis arterio-venous graft design reducing the hemodynamic risk of vascular access dysfunction. J. Biomech. 100, 109591.

Fraser, K.H., Zhang, T., Taskin, M.E., Griffith, B.P. and Wu, Z.J., 2012. A quantitative comparison of mechanical blood damage parameters in rotary ventricular assist devices: shear stress, exposure time and hemolysis index.

Ghodrati, M., Khienwad, T., Maurer, A., Moscato, F., Zonta, F., Schima, H., Aigner, P., 2021. Validation of numerically simulated ventricular flow patterns during left ventricular assist device support. Int. J. Artif. Organs 44 (1), 30–38.

Gil, A., Navarro, R., Quintero, P., Mares, A., 2023. Hemocompatibility and hemodynamic comparison of two centrifugal LVADs: HVAD and HeartMate3. Biomech. Model. Mechanobiol. 22 (3), 871–883.

Goubergrits, L., 2006. Numerical modeling of blood damage: current status, challenges and future prospects. Expert Rev. Med. Devices 3 (5), 527–531.

Guyton, A.C., 1973. Cardiac output and its regulation, W.B. Saunders Company; 2nd edition (12 Jun. 1973) 353-371.

Inamullah, O., Chiang, Y.P., Bishawi, M., Weiss, M., Lutz, M.W., Blue, L.J., Feng, W., Milano, C.A., Luedke, M., Husseini, N.E., 2021. Characteristics of strokes associated with centrifugal flow left ventricular assist devices. Sci. Rep. 11 (1), 1645.

Kirklin, J.K., Naftel, D.C., Kormos, R.L., Pagani, F.D., Myers, S.L., Stevenson, L.W., Acker, M.A., Goldstein, D.L., Silvestry, S.C., Milano, C.A., Baldwin, J.T., 2014. Interagency Registry for Mechanically Assisted Circulatory Support (INTERMACS) analysis of pump thrombosis in the HeartMate II left ventricular assist device. J. Heart Lung Transplant. 33 (1), 12–22.

Khoo, D.P., Cookson, A.N., Gill, H.S., Fraser, K.H., 2018. Normal fluid stresses are prevalent in rotary ventricular assist devices: a computational fluid dynamics analysis. Int. J. Artif. Organs 41 (11), 738–751.

Krabatsch, T., Netuka, I., Schmitto, J.D., Zimpfer, D., Garbade, J., Rao, V., Morshuis, M., Beyersdorf, F., Marasco, S., Damme, L., Pya, Y., 2017. Heartmate 3 fully magnetically levitated left ventricular assist device for the treatment of advanced heart failure–1 year results from the Ce mark trial. J. Cardiothorac. Surg. 12, 1–8.

Medvitz, R.B., Reddy, V., Deutsch, S., Manning, K.B. and Paterson, E.G., 2009. Validation of a CFD methodology for positive displacement LVAD analysis using PIV data.

Mehra, M.R., Goldstein, D.J., Uriel, N., Cleveland Jr, J.C., Yuzefpolskaya, M., Salerno, C., Walsh, M.N., Milano, C.A., Patel, C.B., Ewald, G.A., Itoh, A., 2018. Two-year outcomes with a magnetically levitated cardiac pump in heart failure. N. Engl. J. Med. 378 (15), 1386–1395.

Mehra, M.R., Naka, Y., Uriel, N., Goldstein, D.J., Cleveland Jr, J.C., Colombo, P.C., Walsh, M.N., Milano, C.A., Patel, C.B., Jorde, U.P., Pagani, F.D., 2017. A fully magnetically levitated circulatory pump for advanced heart failure. N. Engl. J. Med. 376 (5), 440–450.

Martorell, J., Santoma, P., Kolandaivelu, K., Kolachalama, V.B., Melgar-Lesmes, P., Molins, J.J., Garcia, L., Edelman, E.R., Balcells, M., 2014. Extent of flow recirculation governs expression of atherosclerotic and thrombotic biomarkers in arterial bifurcations. Cardiovasc. Res. 103 (1), 37–46.

Mori, S., Tretter, J.T., Spicer, D.E., Bolender, D.L., Anderson, R.H., 2019. What is the real cardiac anatomy? Clin. Anat. 32 (3), 288–309.

Nammakie, E., Niroomand-Oscuii, H., Koochaki, M., Ghalichi, F., 2017. Computational fluid dynamics-based study of possibility of generating pulsatile blood flow via a continuous-flow VAD. Med. Biol. Eng. Compu. 55, 167–178.

Oran B., Oran E., 2017. "Endovascular permanent heart assist device", US Patent 9,555,175.

Oran, E., Abo-Serie, E., Jewkes, J., Henry, M., Oran, B., 2024. Design and optimisation of an Intra-Aortic Shrouded rotor axial pump. J. Biomech. 162, 111858.

Puhan, P., Awasthi, A., Mukherjee, A.K., Atta, A., 2021. CFD modeling of segregation in binary solid-liquid fluidized beds: Influence of liquid viscosity and density. Chem. Eng. Sci. 246, 116965.

Quinlan, N.J., Dooley, P.N., 2007. Models of flow-induced loading on blood cells in laminar and turbulent flow, with application to cardiovascular device flow. Ann. Biomed. Eng. 35, 1347–1356.

Raffel, M., Willert, C.E., Scarano, F., Kähler, C.J., Wereley, S.T., Kompenhans, J., 2018. Particle image velocimetry: a practical guide. Springer.

Rogers, J.G., Pagani, F.D., Tatooles, A.J., Bhat, G., Slaughter, M.S., Birks, E.J., Boyce, S. W., Najjar, S.S., Jeevanandam, V., Anderson, A.S., Gregoric, I.D., 2017. Intrapericardial left ventricular assist device for advanced heart failure. N. Engl. J. Med. 376 (5), 451–460.

Santiago, A., Butakoff, C., Eguzkitza, B., Gray, R.A., May-Newman, K., Pathmanathan, P., Vu, V., Vázquez, M., 2022. Design and execution of a verification, validation, and uncertainty quantification plan for a numerical model of left ventricular flow after LVAD implantation. PLoS Comput. Biol. 18 (6), e1010141.

Silva, P.A., Tsoutsanis, P., Antoniadis, A.F., 2021. Simple multiple reference frame for high-order solution of hovering rotors with and without ground effect. Aerosp. Sci. Technol. 111, 106518.

Starling, R.C., Moazami, N., Silvestry, S.C., Ewald, G., Rogers, J.G., Milano, C.A., Rame, J.E., Acker, M.A., Blackstone, E.H., Ehrlinger, J., Thuita, L., 2014. Unexpected abrupt increase in left ventricular assist device thrombosis. N. Engl. J. Med. 370 (1), 33–40.

Thamsen, B., Blümel, B., Schaller, J., Paschereit, C.O., Affeld, K., Goubergrits, L., Kertzscher, U., 2015. Numerical analysis of blood damage potential of the HeartMate II and HeartWare HVAD rotary blood pumps. Artif. Organs 39 (8), 651–659.

Thamsen, B., Gülan, U., Wiegmann, L., Loosli, C., Daners, M.S., Kurtcuoglu, V., Holzner, M., Meboldt, M., 2020. Assessment of the flow field in the HeartMate 3

using three-dimensional particle tracking velocimetry and comparison to computational fluid dynamics. ASAIO J. 66 (2), 173–182.
Wiegmann, L., Thamsen, B., De Zélicourt, D., Granegger, M., Boës, S., Schmid Daners, M., Meboldt, M., Kurtcuoglu, V., 2019. Fluid dynamics in the HeartMate 3: influence of the artificial pulse feature and residual cardiac pulsation. Artif. Organs 43 (4), 363–376.
Wachter, K., Franke, U.F., Rustenbach, C.J., Baumbach, H., 2019. Minimally invasive versus conventional lvad-implantation—an analysis of the literature. Thorac. Cardiovasc. Surg. 67 (03), 156–163.
Xu, L., Yang, M., Ye, L., Dong, Z., 2015. Computational fluid dynamics analysis and PIV validation of a bionic vortex flow pulsatile LVAD. Technol. Health Care 23 (s2).
Zhang, J., Chen, Z., Griffith, B.P., Wu, Z.J., 2020. Computational characterization of flow and blood damage potential of the new maglev CH-VAD pump versus the HVAD and HeartMate II pumps. Int. J. Artif. Organs 43 (10), 653–662.